

Digital Deep Joint Source-Channel Coding with Blind Training for Adaptive Modulation and Power Control

Yongjeong Oh, Joohyuk Park, Jinho Choi, Jihong Park, and Yo-Seb Jeon

Abstract—This paper proposes a novel digital deep joint source-channel coding (DeepJSCC) framework that achieves robust performance across diverse communication environments without requiring extensive retraining and prior knowledge of communication environments. Traditional digital DeepJSCC techniques often face challenges in adapting to various communication environments, as they require significant training overhead and large amounts of communication data to develop either multiple specialized models or a single generalized model, in predefined communication environments. To address this challenge, in our framework, an error-adaptive blind training strategy is devised, which eliminates the need for prior knowledge of communication environments. This is achieved by modeling the relationship between the encoder’s output and the decoder’s input using binary symmetric channels, and optimizing bit-flip probabilities by treating them as trainable parameters. In our framework, a training-aware communication strategy is also presented, which dynamically selects the optimal encoder-decoder pair and transmission parameters based on current channel conditions. In particular, in this strategy, an adaptive power and modulation control method is developed to minimize the total transmission power, while maintaining high task performance. Simulation results demonstrate that our framework outperforms existing DeepJSCC methods, achieving higher peak signal-to-noise ratio, lower power consumption, and requiring significantly fewer encoder-decoder pairs for adaptation.

Index Terms—Joint source-channel coding, semantic communication, blind training, bit-flip probability, adaptive modulation and power control.

I. INTRODUCTION

Semantic communication is a transformative approach to data communication that focuses on conveying the meanings or semantics of raw data relevant to a specific task or goal, rather than accurately transmitting every bit of raw data as in traditional communication [1]–[5]. By sending only essential task-relevant information, it has great potential to enhance bandwidth efficiency and robustness to channel perturbations. A key application is in image and video transmission, where semantic communication extracts semantics through object recognition, scene understanding, and advanced compression algorithms, and transfers perceptually similar content using

minimal bandwidth, even under poor channel conditions [6]–[8]. One of the first methods implementing this idea is the deep joint source-channel coding (DeepJSCC) framework [9]. In DeepJSCC, the communication transceiver is emulated by an encoder-decoder structured deep neural network (DNN), where the encoder jointly performs pre-processing to extract semantics, source encoding, and channel encoding, while the decoder simultaneously handles source decoding, channel decoding, and post-processing for the target task. DeepJSCC has demonstrated its excellence, particularly in challenging scenarios with low signal-to-noise ratios (SNRs) or stringent bandwidth constraints [9]–[12].

Despite its potential, DeepJSCC remains in its nascent stage, with most of existing frameworks relying on analog-like communication architectures that transmit continuous-valued signals over additive noisy channels [9]–[12]. This approach is well-suited for DNNs, which naturally process continuous outputs in their hidden layers, and additive channels can be modeled by a single DNN layer, enabling end-to-end DNN differentiation and trainability. However, this assumption diverges significantly from digital communication systems, limiting the broader adoption and practical deployment of DeepJSCC. To address this limitation, recent studies [13]–[24] have begun exploring ways to integrate DeepJSCC into digital communication systems as we will review next.

A. Digital DeepJSCC: Recent Studies and Limitations

The transition from analog to digital communication systems presents new challenges for DeepJSCC, as digital environments require the handling of discrete bits and symbols. To address this, earlier works focused on mapping the real-valued output of the encoder to discrete symbols or bits to improve compatibility with digital communication architectures [13]–[17]. This approach was further extended by incorporating non-orthogonal multiple access to enhance bandwidth efficiency [18], and lightweight neural network structures were developed to accommodate the limited computational power of edge devices [19].

Despite these advancements, digital DeepJSCC still faces significant challenges, particularly in optimizing power and modulation levels, to achieve high task performance across various communication environments. This multi-dimensional optimization differs from that of analog DeepJSCC, which primarily focuses on power optimization alone. The primary difficulty in addressing this optimization problem is that the relationship between power, modulation, and task performance is

Yongjeong Oh, Joohyuk Park, and Yo-Seb Jeon are with the Department of Electrical Engineering, POSTECH, Pohang, Gyeongbuk 37673, Republic of Korea.

Jinho Choi is with the School of Electrical and Mechanical Engineering, The University of Adelaide, SA 5005, Australia.

Jihong Park is with the Information Systems Technology and Design Pillar, Singapore University of Technology and Design, Singapore 487372.

Yo-Seb Jeon and Jihong Park are corresponding authors (email: yoseb.jeon@postech.ac.kr, jihong_park@sutd.edu.sg).

intractable; thus, it is challenging to derive an analytical optimal solution. Moreover, since the optimal power-modulation pair varies depending on channel conditions, addressing all possible channel conditions requires significant training overhead and large amounts of communication data to develop either multiple specialized models or a single generalized model.

Due to this difficulty, most digital DeepJSCC methods train the semantic encoder and decoder in predefined communication environments where the channel distributions, modulation schemes, or transmission power are predetermined [15]–[21]. In addition, they impose a strict constraint in which the transmitter applies the same power or modulation scheme to all transmitted symbols. As a result, if any communication factors change—such as variations in channel conditions, shifts in modulation schemes, or fluctuations in transmission power—task performance can degrade significantly, as the encoder and decoder, optimized for specific communication conditions, may not generalize well to unexpected environments. Additionally, the strict constraints on modulation and power fail to account for the varying importance or reliability of individual bits, meaning the encoder and decoder may not prioritize critical bits that require higher protection or more robust transmission, further worsening task performance.

Recently, to address this difficulty, a binary symmetric channel (BSC)-based digital DeepJSCC training method was proposed [24], where each transmitted bit experiences different bit-flip probabilities. During the communication stage, the modulation level for each symbol is adjusted based on the channel conditions, while ensuring that the bit-flip error remains below the predefined bit-flip probability used during training. In this strategy, however, the bit-flip probabilities were treated as hyper-parameters, which incurs substantial training overhead in hyper-parameter tuning. Additionally, due to the difficulty of due to the difficulty of jointly optimizing power and modulation, only modulation was adjusted, leading to performance limitations. In addition to digital DeepJSCC methods that consider training, an adaptive modulation method based on pre-trained models was proposed [22]. However, this method does not account for the effects of modulation and fading channels during training, so its task performance is inevitably limited.

B. Contributions and Paper Organization

To overcome these limitations, this paper introduces a novel digital DeepJSCC framework, dubbed *BlindJSCC*, which achieves robust performance across diverse communication environments without the need for extensive retraining or large amounts of data. The proposed framework consists of two strategies: (i) error-adaptive blind training and (ii) training-aware communication. In the error-adaptive blind training strategy, we first model the relationship between the encoder’s output and the decoder’s input using BSCs, which simplifies digital communication into a more manageable form. Next, we optimize the bit-flip probabilities of BSCs by treating them as trainable parameters rather than static values determined

by a specific communication environment. To facilitate this, we employ a continuous relaxation technique that approximates discrete random variables with continuous ones, enabling smooth gradient-based optimization. Further, to adapt to varying channel conditions, we train representative bit-flip probability sets that capture various communication scenarios, including variations in channel conditions, transmission power, and modulation schemes. After performing the proposed training strategy, in the training-aware communication strategy, we select the most suitable bit-flip probability set and corresponding encoder-decoder pair for the given channel condition, total power, and transmission rate constraints. Concurrently, we optimize the power and modulation levels for each transmission symbol to achieve the desired bit-flip probabilities. Our communication strategy utilizes two optimization methods: (i) power optimization, which adjusts transmission power while keeping modulation levels fixed, and (ii) joint modulation and power optimization, which dynamically adjusts both parameters to minimize overall power consumption.

The major contributions of this paper are summarized as follows:

- We present a novel DeepJSCC training method that enables the semantic encoder and decoder to be trained without the need for prior knowledge of communication factors such as channel conditions, transmission power, and modulation schemes.
- We propose a regularization term incorporated into the loss function to train representative bit-flip probability sets. This training is conducted in an end-to-end manner, so that the bit-flip probabilities are jointly trained with the encoder-decoder pair, capturing how the bit-flip errors impact task performance.
- We introduce a communication strategy that adapts to varying communication environments by dynamically selecting the most suitable encoder-decoder pair and adjusting transmission power and modulation levels.
- For image transmission tasks with the MNIST [25], CIFAR-10 [26], and STL-10 [27] datasets, our proposed BlindJSCC achieves up to a 10% improvement in PSNR and reduces total transmission power by up to 70%, at an SNR of 20 dB, compared to other DeepJSCC frameworks.

Note that this work extends its conference version [28] with the following novel contributions. First, unlike [28], which considered a fixed channel condition associated with a single bit-flip probability for each transmitted bit, this work considered a set K of bit-flip probabilities, addressing various channel conditions. Second, while [28] focused on optimizing only transmit power, we jointly optimize both power and modulation in this work. Lastly, we provide extensive simulation results using various datasets and comparisons with other DeepJSCC baseline methods. To differentiate the BlindJSCC version in [28] from the extended version in this paper, we denote the version in [28] as BlindJSCC-P and the extended version as BlindJSCC-MP in the simulation section.

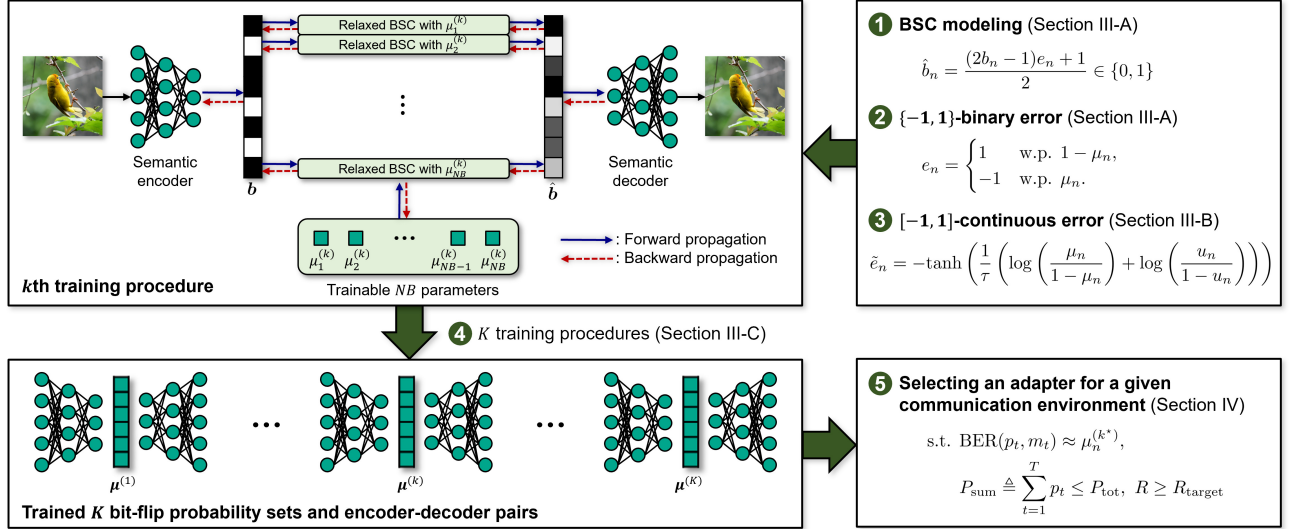


Fig. 1: The training and communication strategies of BlindJSSC with trainable NB parameters and K training procedures.

II. SYSTEM MODEL

We consider a typical digital DeepJSSC system for an image transmission task. Let $\mathbf{u} \in \mathbb{R}^M$ be an image data and $\boldsymbol{\theta}_{\text{enc}}$ be the parameter vector of the encoder. Then, the transmitter encodes the image data as follows:

$$\mathbf{v} = f_{\boldsymbol{\theta}_{\text{enc}}}(\mathbf{u}) \in \mathbb{R}^N, \quad (1)$$

where $f_{\boldsymbol{\theta}_{\text{enc}}}$ is the encoding function, and \mathbf{v} is the semantic feature vector of length N . After the encoding process, the transmitter quantizes each element of \mathbf{v} using a B -bit quantizer. The resulting quantized value is given by

$$q_i = \mathbf{Q}(v_i) \in \mathcal{Q}, \quad i \in \{1, \dots, N\}, \quad (2)$$

where v_i represents the i th element of \mathbf{v} , $\mathcal{Q} = \{\tilde{q}_1, \tilde{q}_2, \dots, \tilde{q}_{2^B}\}$ is the codebook of the quantizer, and $\mathbf{Q} : \mathbb{R} \rightarrow \mathcal{Q}$ is the quantization function. For each codeword \tilde{q}_j , the corresponding bit sequence is determined as $\tilde{\mathbf{b}}_j = \mathbf{B}(\tilde{q}_j) \in \{0, 1\}^B$, where $\mathbf{B} : \mathcal{Q} \rightarrow \{0, 1\}^B$ is a mapping function that converts each codeword \tilde{q}_j into a unique binary sequence of length B . Based on this, the transmitter converts the quantized value q_i of (2) into its corresponding binary sequence, as follows:

$$\mathbf{b}_i = \mathbf{B}(q_i) \in \{0, 1\}^B, \quad i \in \{1, \dots, N\}. \quad (3)$$

After quantizing all elements of \mathbf{v} , the transmitter obtains the bit sequence $\mathbf{b} = [\mathbf{b}_1^T, \dots, \mathbf{b}_N^T]^T \in \{0, 1\}^{NB}$. Then, through a digital modulation process, this bit sequence is converted into a symbol sequence \mathbf{x} of length T .

The transmission rate, representing the average number of transmitted bits per channel use, is defined as

$$R = \frac{NB}{T}, \quad (4)$$

implying how densely the bits are packed for each channel use. To ensure efficient communication, the transmission rate

needs to satisfy or exceed a predefined target transmission rate, denoted as R_{target} , as follows:

$$R \geq R_{\text{target}}. \quad (5)$$

After the modulation process, the transmitter allocates a power p_t to each symbol x_t under the total power constraint, which is given by

$$P_{\text{sum}} \triangleq \sum_{t=1}^T p_t \leq P_{\text{tot}}, \quad (6)$$

where P_{tot} denotes the total available transmission power for transmitting the symbol sequence \mathbf{x} .

The wireless channel between the transmitter and receiver is modeled as a block fading channel, where the channel coefficients remain constant during the coherence time [29]. Under this assumption, the received signal at time slot t is expressed as

$$y_t = h\sqrt{p_t}x_t + n_t, \quad t \in \{1, \dots, T\}, \quad (7)$$

where $h \in \mathbb{C}$ is a complex-valued channel coefficient, and $n_t \sim \mathcal{CN}(0, \sigma^2)$ represents the additive white Gaussian noise (AWGN). The maximum achievable SNR is defined as

$$\text{SNR}_{\text{max}} = 10 \log_{10} \frac{P_{\text{tot}} \mathbb{E}[\gamma]}{NB}, \quad (8)$$

where $\gamma = \frac{|h|^2}{\sigma^2}$ is the channel-gain-to-noise-power ratio. Assume that the channel coefficient h is accurately estimated at the receiver using pilot-assisted channel estimation during each channel coherence time. Then, the receiver performs channel equalization on the received signal in (7), resulting in the equalized signal at time slot t :

$$\tilde{y}_t = \frac{h^*}{|h|^2} y_t = \sqrt{p_t} x_t + \tilde{n}_t, \quad t \in \{1, \dots, T\}, \quad (9)$$

where h^* is the complex conjugate of h , and $\tilde{n}_t = h^* n_t / |h|^2$.

After this, the receiver recovers the estimated symbol sequence $\hat{\mathbf{x}}$, followed by demodulation to determine the estimated bit sequence $\hat{\mathbf{b}} = [\hat{\mathbf{b}}_1^T, \dots, \hat{\mathbf{b}}_N^T]^T \in \{0, 1\}^{NB}$.

After reconstructing the bit sequence, the receiver determines the estimated quantized value by performing the inverse process of \mathcal{B} , as follows:

$$\hat{q}_i = \mathcal{B}^{-1}(\hat{\mathbf{b}}_i) \in \mathcal{Q}, \quad i \in \{1, \dots, N\}, \quad (10)$$

where $\mathcal{B}^{-1} : \{0, 1\}^B \rightarrow \mathcal{Q}$. Once the quantized values are obtained, the receiver can reconstruct the original image data using a semantic decoder parameterized by θ_{dec} . This decoding operation is denoted as

$$\hat{\mathbf{u}} = f_{\theta_{\text{dec}}}(\hat{\mathbf{q}}) \in \mathbb{R}^K. \quad (11)$$

To evaluate the reconstruction quality, we mainly use the peak SNR (PSNR) defined as

$$\text{PSNR} = 10 \log_{10} \left(\frac{\text{MAX}^2}{\text{MSE}} \right), \quad (12)$$

where MAX represents the maximum possible pixel value of the image (e.g., 255 for 8-bit image), and MSE is the mean-squared-error (MSE) between the original and reconstructed images, i.e., $\text{MSE} = \frac{1}{M} \mathbb{E}[\|\mathbf{u} - \hat{\mathbf{u}}\|^2]$.

It should be noted that in this paper, we do not delve into the design and optimization of the quantization-related functions \mathcal{Q} , \mathcal{B} , and \mathcal{B}^{-1} ; thereby, we assume that these functions are predefined and consistent across the entire process, by employing well-established quantization methods (e.g., [30]–[32]). In this context, we simply employ the uniform quantizer defined as

$$q_i = \mathcal{Q}(v_i) = \Delta \cdot \left\lfloor \frac{v_i - v_{\min}}{\Delta} + \frac{1}{2} \right\rfloor + v_{\min}, \quad (13)$$

where v_{\min} and v_{\max} are the minimum and maximum values of quantized values, respectively, and $\Delta = \frac{v_{\max} - v_{\min}}{2^B - 1}$. The relationship between q_i and \mathbf{b}_i is given by

$$q_i = v_{\min} + \Delta \sum_{k=1}^B 2^{k-1} b_i^{(k)}, \quad (14)$$

where $b_i^{(k)}$ is the k th element of \mathbf{b}_i .

In this paper, we propose a novel digital DeepJSCC framework named BlindJSCC. Traditional DeepJSCC methods often struggle to adapt to diverse communication environments because their training requires substantial overhead and large amounts of communication data to create either multiple specialized models or a single generalized model for predefined communication conditions. BlindJSCC addresses these issues by introducing an error-adaptive blind training strategy, which eliminates the need for prior knowledge of communication factors. Furthermore, it incorporates a training-aware communication strategy that dynamically adjusts transmission parameters based on varying channel conditions. In Section III, we discuss the training strategy of BlindJSCC in detail, and in Section IV, we explain its communication strategy. The high-

level procedure of BlindJSCC is summarized in Fig. 1.

III. ERROR-ADAPTIVE BLIND TRAINING STRATEGY OF BLINDJSCC

In this section, we introduce an error-adaptive blind training strategy of BlindJSCC, which allows the semantic encoder and decoder to be trained without prior knowledge of communication factors such as channel conditions, transmission power, and modulation scheme.

A. BSC Modeling

The core concept behind our training strategy stems from a stochastic channel model that captures various communication processes, including modulation and fading channels, in an integrated manner, rather than treating each process separately. Specifically, our training strategy simplifies the complex transmission and reception processes of NB bits in digital communication systems to a more manageable form by modeling their combined effects using NB BSCs. Then, for the n th BSC, where $n \in \{1, \dots, NB\}$, the relationship between the transmitted n th bit b_n and the corresponding received bit \hat{b}_n is modeled as follows:

$$\hat{b}_n = \frac{(2b_n - 1)e_n + 1}{2} \in \{0, 1\}, \quad (15)$$

where $e_n \in \{-1, 1\}$ is a binary error determined as

$$e_n = \begin{cases} 1, & \text{w.p. } 1 - \mu_n, \\ -1, & \text{w.p. } \mu_n, \end{cases} \quad (16)$$

and $\mu_n \in (0, 0.5)$ represents the bit-flip probability for the n th BSC. Note that μ_n plays a crucial role in characterizing the various processes in digital communication systems. For example, if the n th bit is transmitted in the t th symbol x_t using 2^{m_t} -QAM with transmission power p_t over a fading channel, the bit-flip probability μ_n for the ML detection can be approximated as follows [33]:

$$\begin{aligned} \mu_n \approx & \frac{\sqrt{2^{m_t}} - 1}{\sqrt{2^{m_t}} \log_2 \sqrt{2^{m_t}}} \text{erfc} \left(\sqrt{\frac{3p_t \gamma}{2(2^{m_t} - 1)}} \right) \\ & + \frac{\sqrt{2^{m_t}} - 2}{\sqrt{2^{m_t}} \log_2 \sqrt{2^{m_t}}} \text{erfc} \left(3 \sqrt{\frac{3p_t \gamma}{2(2^{m_t} - 1)}} \right), \end{aligned} \quad (17)$$

where $\text{erfc}(x) = 1 - \frac{2}{\sqrt{\pi}} \int_0^x \exp(-u^2) du$ is the complementary error function, which is a function of several key factors in digital communication systems, including transmission power p_n , channel-gain-to-noise-power ratio γ , and modulation level m_n .

A key advantage of BSC modeling is its ability to unify the modeling for diverse and unpredictable digital communication systems. This modeling also facilitates end-to-end learning for the semantic encoder and decoder by regarding the linear equation in (15) as a layer of a DNN [13]. However, when employing this modeling, it is crucial to determine the bit-flip probabilities $\{\mu_n\}_{n=1}^{NB}$, as they significantly influence the

performance of image reconstruction during training. One of the primary challenges in determining these bit-flip probabilities is that the relationship between μ_n and reconstruction performance is intricate and intractable, making it difficult to derive an analytical optimal solution. Most existing digital DeepJSCC methods have failed to account for this relationship, as their training is typically performed in a specific communication environment, where all symbols are assumed to experience the same bit-flip probability. Another challenge lies in adapting to diverse communication environments. Even if $\{\mu_n\}_{n=1}^{NB}$ are properly determined, certain digital communication systems may struggle to achieve these bit-flip probabilities due to constraints on total power or transmission rate.

To address these challenges, in our training strategy, we introduce the end-to-end learning-based parametric training approach. In this approach, the bit-flip probabilities $\{\mu_n\}_{\forall n}$ are treated as *trainable parameters*, rather than fixed constants predetermined by a specific communication environment. This implies that our training approach eliminates the need for explicit knowledge of communication factors, thereby significantly reducing training overhead and the necessity for extensive communication data collection. Further, by incorporating the bit-flip probabilities into the training process, our approach enables their joint optimization alongside the semantic encoder and decoder.

To further elaborate on our parametric training approach, we start by defining a trainable raw parameter vector, $\tilde{\boldsymbol{\mu}} = [\tilde{\mu}_1, \tilde{\mu}_2, \dots, \tilde{\mu}_{NB}]^T \in \mathbb{R}^{NB}$. Then, we transform these raw parameters to represent the bit-flip probabilities as follows:

$$\mu_n = \frac{\text{Sigmoid}(\mu'_n)}{2}, \quad \forall n, \quad (18)$$

where $\text{Sigmoid}(x) = \frac{1}{1+e^{-x}}$ is the sigmoid function. This transformation ensures that the μ_n falls within the appropriate bit-flip probability range $(0, 0.5)$.

In the following subsections, we elaborate a more detailed exploration for training the bit-flip probabilities in (18). Specifically, in Sec. III-B, we focus on deriving the gradient for μ_n to enable end-to-end learning. Then, in Sec. III-C, we describe the loss function that guides $\{\mu_n\}_{\forall n}$ to converge to the appropriate values, along with the training method designed to ensure effective adaptation to diverse communication environments.

B. End-to-End Learning via Continuous Relaxation

The primary challenge in computing the gradient for μ_n arises from the discrete nature of the BSC described in (15). Specifically, since the binary error e_n in (16) follows a *discrete* Bernoulli distribution with μ_n , it is non-trivial to calculate the gradient for μ_n . To facilitate the training of μ_n , our training strategy employs the continuous relaxation method in [34], which effectively approximates discrete random variables with their continuous counterparts. A representative example of this method is the relaxation of the max function in the Gumbel-max trick to a softmax function, commonly known as the Gumbel-softmax trick.

Leveraging the continuous relaxation in [34], the binary error e_n in (16) is approximated by its continuous counterpart, given by

$$\tilde{e}_n = -\tanh\left(\frac{1}{\tau}\left(\log\left(\frac{\mu_n}{1-\mu_n}\right) + \log\left(\frac{u_n}{1-u_n}\right)\right)\right), \quad (19)$$

where u_1, \dots, u_{NB} are independent and identically distributed random variables, each following the uniform distribution $\mathcal{U}(0, 1)$, and $\tau \geq 0$ is the temperature parameter. The detailed derivation of (19) can be obtained by applying a linear transformation to the Bernoulli random variable described in [34]. In contrast to the binary error e_n , its continuous counterpart \tilde{e}_n is differentiable with respect to μ_n . The corresponding gradient is given by

$$\begin{aligned} \frac{\partial \tilde{e}_n}{\partial \mu_n} &= -\text{sech}^2\left(\frac{1}{\tau}\left(\log\left(\frac{\mu_n}{1-\mu_n}\right) + \log\left(\frac{u_n}{1-u_n}\right)\right)\right) \\ &\quad \times \frac{1}{\tau \mu_n (1-\mu_n)}, \end{aligned} \quad (20)$$

where $\text{sech}(x) = \frac{2}{e^x + e^{-x}}$. With this continuous relaxation, substituting \tilde{e}_n into e_n relaxes the input-output relationship of the BSC model in (15) as follows:

$$\hat{b}_n = \frac{(2b_n - 1)\tilde{e}_n + 1}{2} \in [0, 1]. \quad (21)$$

In our training strategy, the relaxed BSC is treated as a layer within the DNN. This integration enables the computation of gradients for the semantic encoder, bit-flip probabilities, and semantic decoder, thereby allowing end-to-end learning for all trainable parameters. Specifically, let \mathcal{L} be the loss function computed at the output of the semantic decoder, which will be detailed in Sec. III-C. Then, utilizing the chain rule, the gradient of the loss with respect to μ_n becomes

$$\frac{\partial \mathcal{L}}{\partial \mu_n} = \frac{\partial \mathcal{L}}{\partial \hat{b}_n} \cdot \frac{\partial \hat{b}_n}{\partial \tilde{e}_n} \cdot \frac{\partial \tilde{e}_n}{\partial \mu_n}, \quad (22)$$

where the first component $\frac{\partial \mathcal{L}}{\partial \hat{b}_n}$ can be obtained by performing backpropagation at the semantic decoder. The second component is obtained from the relaxed BSC, given by $\frac{\partial \hat{b}_n}{\partial \tilde{e}_n} = b_n - \frac{1}{2}$. Following the similar procedure above, the gradient for the semantic encoder is determined as

$$\frac{\partial \mathcal{L}}{\partial \boldsymbol{\theta}_{\text{enc}}} = \sum_{n=1}^{NB} \frac{\partial \mathcal{L}}{\partial \hat{b}_n} \cdot \frac{\partial \hat{b}_n}{\partial b_n} \cdot \frac{\partial b_n}{\partial \boldsymbol{\theta}_{\text{enc}}}, \quad (23)$$

where the second term is derived from the relaxed BSC, given by $\frac{\partial \hat{b}_n}{\partial b_n} = \tilde{e}_n$. For other trainable parameters, the gradients $\frac{\partial \mathcal{L}}{\partial \mu'_n}$ and $\frac{\partial \mathcal{L}}{\partial \boldsymbol{\theta}_{\text{dec}}}$, are readily computed by performing backpropagation with the chain rule. Meanwhile, in practice, these gradients can be computed using automatic differentiation techniques provided by modern deep learning frameworks, such as TensorFlow and Pytorch. Therefore, our gradient computation is not overly complex, enabling ease of implementation and efficient optimization.

C. Regularization for Optimizing μ_n in End-to-End Learning

The major challenge in training μ_n is its tendency to converge to very small values, particularly when the loss function is designed to minimize the reconstruction error only, such as MSE. This vanishing phenomenon arises because the reconstruction error tends to decrease with lower bit-flip probabilities. To address this challenge, we incorporate a regularization term into the loss function, as follows:

$$\mathcal{L} = \mathbb{E}_{\mathbf{u}, \hat{\mathbf{u}}} [d(\mathbf{u}, \hat{\mathbf{u}})] + \lambda \mathcal{R}(\boldsymbol{\mu}), \quad (24)$$

where $d(\mathbf{u}, \hat{\mathbf{u}})$ is a distortion measure between the original input image \mathbf{u} and its reconstruction $\hat{\mathbf{u}}$, $\lambda > 0$ is a regularization weight that controls the strength of the regularization, and $\mathcal{R}(\boldsymbol{\mu})$ represents a regularization term that encourages the parameter μ_n to converge to larger values by penalizing it when its value is small. A representative example of our loss function is a combination of MSE and L2-based regularization, formulated as

$$\mathcal{L} = \frac{1}{M} \mathbb{E}_{\mathbf{u}, \hat{\mathbf{u}}} [\|\mathbf{u} - \hat{\mathbf{u}}\|^2] + \frac{\lambda}{NB} \sum_{n=1}^{NB} \left(\frac{1}{2} - \mu_n \right)^2, \quad (25)$$

where the second term, representing L2 regularization, penalizes deviations of $\{\mu_n\}_{\forall n}$ from their maximum value 0.5.

In our loss function of (24), increasing λ causes the average value of $\boldsymbol{\mu}$ to converge toward higher values due to the greater significance of the regularization term. This increase, however, is attained at the cost of increased distortion, as the training procedure places more emphasis on accommodating challenging communication environments rather than minimizing distortion. Therefore, our training strategy involves a trade-off between accommodating challenging communication environments and achieving high task performance.

Based on the trade-off above, our key idea for effectively adapting to diverse communication environments is to represent these environments using K distinct bit-flip probability sets. Each set is characterized by a different average bit-flip probability and covers a wide range of communication scenarios. Specifically, a set with a low average bit-flip probability can represent favorable communication environments, such as those with high total power or strong channel conditions. On the other hand, a set with a high average bit-flip probability represents more challenging communication environments with poor channel conditions or low total power. Recall that our approach leverages the fact that the bit-flip probability encapsulates the key factors in digital communication systems, including channel, power, and modulation levels, as shown in (17). As a result, we can significantly reduce the training overhead and the number of models compared to traditional DeepJSCC methods, which require separate models for each combination of communication parameters.

Let $\boldsymbol{\mu}^{(k)}$ be the k th bit-flip probability set, where $k \in \{1, \dots, K\}$. Then, based on the loss function in (24), our training strategy performs K training procedures, each with a different regularization strength, λ_k , $k \in \{1, \dots, K\}$, such

TABLE I: Comparison of the PSNRs for task-based and L2-based regularizations across varying $\tilde{\mu}^{(1)}$ and λ_1 values at $\text{SNR}_{\max} \in \{10, 20\}$ dB on the MNIST dataset.

SNR _{max} = 10 dB		λ_1			
		10^{-4}	10^{-3}	10^{-2}	
Target-based regularization	$\tilde{\mu}^{(1)}$	0.1	34.47	35.06	36.08
		0.2	34.41	35.74	36.08
		0.3	35.05	35.99	35.49
L2-based regularization		35.31	36.12	33.74	
SNR _{max} = 20 dB		λ_1			
		10^{-4}	10^{-3}	10^{-2}	
Target-based regularization	$\tilde{\mu}^{(1)}$	0.1	42.03	42.04	41.32
		0.2	41.93	41.82	39.69
		0.3	42.11	41.45	38.25
L2-based regularization		42.09	40.70	35.56	

that $\lambda_1 < \dots < \lambda_K$. This results in K different bit-flip probability sets and corresponding encoder-decoder pairs. By leveraging these trained bit-flip probability sets, the transmitter and receiver can dynamically select the most suitable encoder-decoder pair for the given communication environment. In Sec. IV, we will provide detailed instructions on how to implement this dynamic selection process.

Meanwhile, the design of the regularization term $\mathcal{R}(\cdot)$ plays a crucial role in ensuring that the K bit-flip probability sets $\{\boldsymbol{\mu}^{(k)}\}_{k=1}^K$ accommodate various communication environments. One intuitive approach would be to set a target value for the k th bit-flip probability set, denoted as $\tilde{\mu}^{(k)}$, and formulate the regularization term as $\mathcal{R}(\boldsymbol{\mu}^{(k)}) = \sum_{n=1}^{NB} (\tilde{\mu}^{(k)} - \mu_n^{(k)})^2$, where $\tilde{\mu}^{(k)}$. While this target-based regularization provides controllability over $\mu_n^{(k)}$'s convergence toward the target value, the relationship between the task performance and the target value is unknown, making the target value a hyperparameter. For this reason, this regularization introduces two hyperparameters, $\boldsymbol{\mu}^{(k)}$ and λ_k . Compared to target-based regularization, the L2-based regularization in (25) simplifies the training process by utilizing a single hyperparameter λ_k . To assess the task performance of both regularizations, we have conducted an experiment on the MNIST dataset under varying $\tilde{\mu}^{(1)}$ and λ_1 values with $K = 1$. Table I shows that after hyperparameter tuning, both the L2-based and target-based regularizations achieve comparable PSNR performance. However, the L2-based regularization achieves this performance using only one hyperparameter, while the target-based regularization requires tuning two parameters. This result implies that optimizing a single hyperparameter, as in the L2-based regularization, appears to be sufficient to achieve high task performance across various communication environments.

Remark 1 (Impact of Regularization Weight λ_k on $\boldsymbol{\mu}^{(k)}$): We analyze the convergence behavior of the average value of $\boldsymbol{\mu}^{(k)}$ in response to changes in the regularization weight λ_k , using a numerical example. In this simulation, we consider an image reconstruction task using the MNIST dataset. All values of $\boldsymbol{\mu}^{(k)}$ are initialized to 0.1, and the loss function in (25) is employed. Fig. 2 shows that as λ_k increases, the average value of $\boldsymbol{\mu}^{(k)}$ converges to higher values. This indicates that more challenging communication environments can be

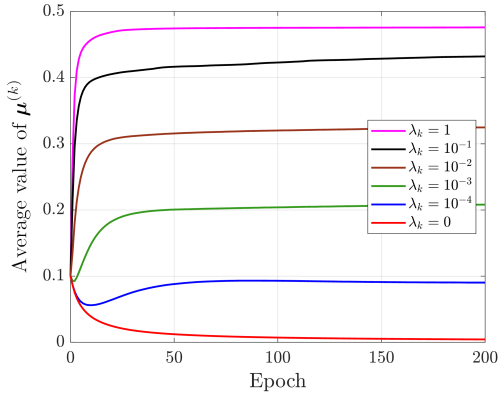


Fig. 2: Convergence behavior of the average value of bit-flip probabilities $\mu^{(k)}$ for different regularization weight λ_k .

effectively captured by increasing λ_k . Fig. 2 also shows that when $\lambda_k = 0$, the average value of $\mu^{(k)}$ converges to a very small value, requiring impractically high transmission power or communication resources to achieve such low bit-flip probabilities.

IV. TRAINING-AWARE COMMUNICATION STRATEGY OF BLINDJSCC

In this section, we optimize a communication strategy to align the actual BERs with the pre-trained bit-flip probabilities, while determining the most suitable encoder-decoder pair.

A. Overview

Suppose that the semantic communication system has the total transmission power constraint, P_{tot} , and the target transmission rate, R_{target} . In our strategy, we consider uncoded QAM to avoid the additional complexity and redundancy introduced by channel encoding and decoding. Based on this, the transmitter and receiver select the most suitable encoder-decoder pair from the K pre-trained pairs, while determining the transmission power and modulation level for each symbol based on the pre-trained K bit-flip probability sets and the current channel-gain-to-noise-power ratio, γ . This channel-adaptive selection and optimization process is denoted as

$$\{k^*, \{p_t, m_t\}_{t=1}^T\} = f_{\text{adapt}}(P_{\text{tot}}, R_{\text{target}}, \{\mu^{(k)}\}_{k=1}^K, \gamma), \quad (26)$$

where k^* is the index of the selected encoder-decoder pair, and f_{adapt} is the adaptation function, which will be detailed in Sec. IV-B and Sec. IV-C. Note that the function f_{adapt} needs to satisfy the transmission rate in (5) and the total power constraint in (6). Moreover, this function should satisfy the BER matching condition that the BER, achieved through the transmission power p_t and modulation level m_t of the t th

symbol carrying the n th bit, closely matches the n th element of $\mu^{(k^*)}$, as follows:

$$\begin{aligned} \mu_n^{(k^*)} &\approx \frac{\sqrt{2^{m_t}} - 1}{\sqrt{2^{m_t}} \log_2 \sqrt{2^{m_t}}} \operatorname{erfc} \left(\sqrt{\frac{3p_t \gamma}{2(2^{m_t} - 1)}} \right) \\ &+ \frac{\sqrt{2^{m_t}} - 2}{\sqrt{2^{m_t}} \log_2 \sqrt{2^{m_t}}} \operatorname{erfc} \left(3 \sqrt{\frac{3p_t \gamma}{2(2^{m_t} - 1)}} \right) \\ &\triangleq \operatorname{BER}(p_t, m_t, \gamma), \end{aligned} \quad (27)$$

where the approximation follows from (17). This condition helps minimize the discrepancy between the bit error rates observed during training and those encountered during communication, leading to improved reliability and task performance. The optimization problem solved by f_{adapt} is summarized as follows:

$$\begin{aligned} (\mathbf{P0}) \quad (k^*, \{p_t, m_t\}_{t=1}^T) &= \operatorname{argmin}_{k, \{p_t^{(k)}, m_t^{(k)}\}_{t=1}^T} \mathbb{E}[d(\mathbf{u}, \hat{\mathbf{u}})], \quad (28) \\ \text{s.t.} \quad &|\operatorname{BER}(p_t^{(k)}, m_t^{(k)}, \gamma) - \mu_n^{(k)}| \leq \epsilon, \\ &\sum_{t=1}^T p_t^{(k)} \leq P_{\text{tot}}, \quad R \geq R_{\text{target}}, \end{aligned}$$

where $p_t^{(k)}$ and $m_t^{(k)}$ represent the power and modulation level for the t th symbol in the k th bit-flip probability set, and $\epsilon \ll 1$. Note that $d(\mathbf{u}, \hat{\mathbf{u}})$ represents the distortion measure between the original input image \mathbf{u} and its reconstruction $\hat{\mathbf{u}}$, used during training, and it decreases as k increases due to the trade-off between adapting to challenging communication environments and maintaining high task performance, as discussed in Sec. III-C.

Once the process above is completed, the transmitter encodes the image data using the selected k^* th encoder, and performs the quantization process to obtain the bit sequence \mathbf{b} . Then, the transmitter transmits \mathbf{b} using the specified modulation levels and transmission powers. It should be noted that the process in (26) is also executed at the receiver. Consequently, with the knowledge of $\{p_t, m_t\}_{t=1}^T$, the receiver can perform the detection to obtain the estimated bit sequence $\hat{\mathbf{b}}$.

In our communication strategy, a proper design of the adaptation function in (26) is crucial for solving the problem $\mathbf{P0}$. In the remainder of this section, we first introduce the adaptive power control (APC) method (see Sec. IV-B) and then explore a more advanced adaptive modulation and power control (AMPC) method (see Sec. IV-C). The overall procedure of our communication strategy is illustrated in Fig. 3.

B. APC Method

The APC method in our communication strategy involves fixing the modulation level and determining the transmission power for each symbol. Specifically, the modulation level is set to the lowest level that satisfies the transmission rate constraint,

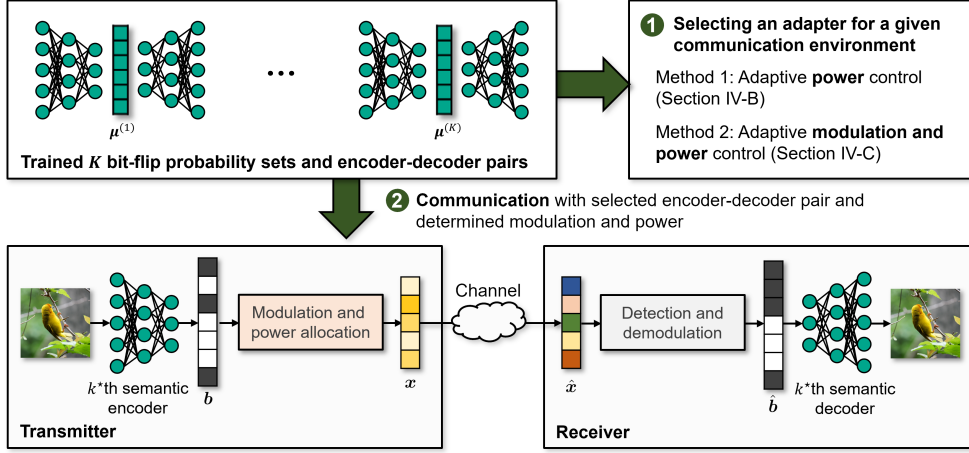


Fig. 3: The overall procedure of the training-aware communication strategy in BlindJSCC with two adaptive control methods.

as follows:

$$m_t^{(k)} = \min \left\{ m : \left\lceil \frac{NB}{m} \right\rceil \leq \frac{NB}{R_{\text{target}}}, m \in \{2, 4, 6, \dots\} \right\} \triangleq m_{\text{APC}}, \quad (29)$$

for all t, k , where $\lceil \frac{NB}{m} \rceil$ represents the length of the symbol sequence T when using 2^m -QAM, and $\frac{NB}{R_{\text{target}}}$ indicates the minimum required length of the symbol sequence to achieve the target transmission rate R_{target} . By setting the modulation level to the minimum value, we reduce the required transmission power by leveraging the fact that higher modulation levels require greater transmission power to satisfy the BER condition in (27). Additionally, this setting simplifies the problem **P0** by ensuring that the constraint $R \geq R_{\text{target}}$ is always satisfied. In this context, the APC method solves the following optimization problem:

$$\begin{aligned} (\mathbf{P1}) \quad & (k^*, \{p_t\}_{t=1}^T) = \underset{k, \{p_t^{(k)}\}_{t=1}^T}{\text{argmin}} \mathbb{E}[d(\mathbf{u}, \hat{\mathbf{u}})], \quad (30) \\ \text{s.t.} \quad & |\text{BER}(p_t^{(k)}, m_{\text{APC}}, \gamma) - \mu_n^{(k)}| \leq \epsilon, \quad \sum_{t=1}^T p_t^{(k)} \leq P_{\text{tot}}. \end{aligned}$$

To solve the problem **P1**, the APC method first sorts the bit-flip probabilities $\{\mu_n^{(k)}\}_{\forall n}$ in ascending order and divides them into $T = \lceil \frac{NB}{m_{\text{APC}}} \rceil$ groups. Next, the method computes the average bit-flip probability for each group as follows:

$$\bar{\mu}_t^{(k)} = \frac{1}{m_{\text{APC}}} \sum_{n \in \mathcal{K}_t} \mu_n^{(k)}, \quad (31)$$

for $t \in \{1, \dots, T\}$, where \mathcal{K}_t is the index set of the t th group. The required transmission power to achieve $\bar{\mu}_t^{(k)}$, denoted as $p_t^{(k)}$, is then determined by solving the equation below:

$$\bar{\mu}_t^{(k)} = \text{BER}(p_t^{(k)}, m_{\text{APC}}, \gamma). \quad (32)$$

In general, since the BER function is monotonically decreasing with respect to $p_t^{(k)}$ for a given m_{APC} , one can readily obtain the solution using various numerical methods such as bisection

or Newton-Raphson algorithms [35]. Further, it should be noted that by sorting $\mu_n^{(k)}$ and averaging similar values, we can assume that $\bar{\mu}_t^{(k)} \approx \mu_n^{(k)}, \forall n \in \mathcal{K}_t$; thereby, the condition in (27) is satisfied by solving the equation of (32). After computing the power $p_t^{(k)}$ for each t and k , the required total power for the k th encoder-decoder pair is obtained as

$$P_{\text{sum}}^{(k)} = \sum_{t=1}^T p_t^{(k)}. \quad (33)$$

Then, to achieve the highest performance while satisfying the power constraint, the index of the most suitable encoder-decoder pair is determined as

$$k^* = \min\{k : P_{\text{sum}}^{(k)} \leq P_{\text{tot}}\}. \quad (34)$$

The corresponding transmission power is set to $p_t = p_t^{(k^*)}$.

After determining k^* , the transmitted bits are sorted to match the order of their corresponding $\mu_n^{(k^*)}$ values, and then modulation and power allocation are performed using m_t and p_t . On the receiver-side, the estimated bits are reordered to their original positions following the demodulation process. Note that these ordering procedures do not incur any additional communication overhead because the sorting operation for $\mu_n^{(k^*)}$ can be performed locally at the transmitter and receiver.

A key feature of the APC method is its simplicity and efficiency in determining modulation levels and transmission powers without complex optimization processes. However, by fixing the modulation level uniformly across all symbols, the method fails to take the performance gains that can be obtained through jointly optimizing the modulation level and transmission power. Consequently, the overall communication efficiency and performance remain constrained. This limitation motivates us to develop a more advanced adaptation method, namely the AMPC method, described in the following subsection.

C. AMPC Method

A primary goal of the proposed AMPC method is to minimize the total transmission power over the APC method, while

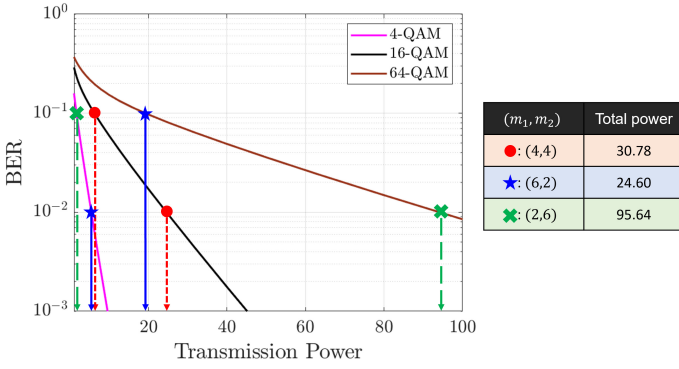


Fig. 4: Comparison of total power for various combinations of modulation levels.

strictly adhering to the transmission rate constraint and BER matching condition. To achieve this goal, our method aims to find the optimal modulation level and corresponding transmission power for each symbol. The corresponding optimization problem is expressed as

$$\begin{aligned}
 (\mathbf{P2}) \quad & (k^*, \{p_t, m_t\}_{t=1}^T) \\
 & = \underset{k, \{p_t^{(k)}, m_t^{(k)}\}_{t=1}^T}{\operatorname{argmin}} \mathbb{E}[d(\mathbf{u}, \hat{\mathbf{u}})] + \nu \sum_{t=1}^T p_t^{(k)}, \quad (35) \\
 & \text{s.t. } |\operatorname{BER}(p_t^{(k)}, m_t^{(k)}, \gamma) - \mu_n^{(k)}| \leq \epsilon, \\
 & \sum_{t=1}^T p_t^{(k)} \leq P_{\text{tot}}, \quad R \geq R_{\text{target}},
 \end{aligned}$$

where $\nu > 0$ is a small constant that ensures $\mathbb{E}[d(\mathbf{u}, \hat{\mathbf{u}})] \gg \nu \sum_{t=1}^T p_t^{(k)}, \forall k$, emphasizing the importance of minimizing distortion while still considering power consumption. To explore this problem more clearly, let us consider the example where the bit sequence length is 16 and the desired symbol sequence length is 4, implying the $R_{\text{target}} = 4$. In this example, the potential combinations of $\{m_1^{(k)}, m_2^{(k)}, m_3^{(k)}, m_4^{(k)}\}$ are $\{8, 4, 2, 2\}$, $\{6, 6, 2, 2\}$, $\{6, 4, 4, 2\}$, $\{4, 4, 4, 4\}$, along with all permutations of these elements. Then, in this example, the optimal combination can be determined by evaluating both the total transmission power and the corresponding distortion.

The main challenge in solving the optimization problem **P2** lies in its non-convexity, which arises from the discrete nature of the modulation level m_n and the non-convexity of the BER function with respect to two variables p_n and m_n . Furthermore, due to the vast number of possible combinations of modulation levels and powers, the domain space can be significantly large. As a result, traditional optimization techniques, and even exhaustive search methods, are highly impractical for finding the optimal solution. To address these challenges, we propose the AMPC method that iteratively optimizes the transmission power and modulation level for each symbol, effectively navigating the complex search space to find near-optimal solutions.

The fundamental idea of the AMPC method is to assign a

Algorithm 1 Adaptive Modulation and Power Control (AMPC) Method

- 1: Set the initial value of m_t , denoted as m_{init} , from (29), $\forall t$.
- 2: Sort μ_n in ascending order.
- 3: $\ell_s = 1, \ell_e = m_{\text{init}}$.
- 4: $h_s = NB - m_{\text{init}} - 1$, and $h_e = NB$.
- 5: $t = 1$
- 6: **while** $t \leq \lfloor \frac{T}{2} \rfloor$
- 7: $m_\ell = \ell_e - \ell_s + 1$ and $m_h = h_e - h_s + 1$.
- 8: $m'_\ell = m_\ell - 2$ and $m'_h = m_h + 2$.
- 9: $\bar{\mu}_\ell = \frac{1}{m_\ell} \sum_{n=\ell_s}^{n=\ell_e} \mu_n$ and $\bar{\mu}_h = \frac{1}{m_h} \sum_{n=h_s}^{n=h_e} \mu_n$.
- 10: $\bar{\mu}'_\ell = \frac{1}{m'_\ell} \sum_{n=\ell_s}^{n=\ell_e-2} \mu_n$ and $\bar{\mu}'_h = \frac{1}{m'_h} \sum_{n=h_s-2}^{n=h_e} \mu_n$.
- 11: Compute powers $p_\ell, p'_\ell, p_h, p'_h$ by solving $\bar{\mu}_\ell = \operatorname{BER}(p_\ell, m_\ell, \gamma), \bar{\mu}'_\ell = \operatorname{BER}(p'_\ell, m'_\ell, \gamma), \bar{\mu}_h = \operatorname{BER}(p_h, m_h, \gamma), \bar{\mu}'_h = \operatorname{BER}(p'_h, m'_h, \gamma)$.
- 12: $p_{\text{sum}} = p_\ell + p_h$ and $p'_{\text{sum}} = p'_\ell + p'_h$.
- 13: **if** ($p'_{\text{sum}} > p_{\text{sum}}$) or ($m_\ell = m_{\text{min}}$) or ($m_h = m_{\text{max}}$)
- 14: $m_t = m_\ell$ and $m_{T-t+1} = m_h$.
- 15: $p_t = p_\ell$ and $p_{T-t+1} = p_h$.
- 16: $\ell_s = \ell_e + 1$ and $h_e = h_s - 1$.
- 17: $\ell_e = \ell_s + m_{\text{init}} - 1$ and $h_s = h_e - m_{\text{init}} + 1$.
- 18: $t = t + 1$.
- 19: **continue**.
- 20: **end**
- 21: **if** $p'_{\text{sum}} \leq p_{\text{sum}}$
- 22: $m_t = m_\ell - 2$ and $m_{T-t+1} = m_h + 2$.
- 23: $p_t = p'_\ell$ and $p_{T-t+1} = p'_h$.
- 24: $\ell_e = \ell_e - 2$ and $h_s = h_s - 2$.
- 25: **end**
- 26: **end**

low modulation level to bits with low bit-flip probabilities, and a high modulation level to bits with higher bit-flip probabilities. The effectiveness of this idea can be verified through a simple example in which two bits need to be transmitted with bit-flip probabilities $\mu_1 = 10^{-1}$ and $\mu_2 = 10^{-2}$, respectively, and the channel-gain-to-noise-power ratio γ is set to be one. Then, we examine three combinations of modulation levels $\{m_1, m_2\}$: (i) $\{4, 4\}$, (ii) $\{6, 2\}$, and (iii) $\{2, 6\}$, each achieving the same transmission rate. Fig. 4 demonstrates the effectiveness of our idea, where the second combination achieves the lowest total transmission power. Furthermore, based on this result, it can be naturally inferred that as the difference between μ_1 and μ_2 increases, the total power gap between the first combination and the others also widens.

The proposed AMPC method, motivated by the key observation mentioned above, is summarized in **Algorithm 1**, where the index k is omitted for the sake of simplicity. The major steps of the algorithm are elaborated below. In Step 1, the initial modulation level is set to the same as in the APC method, ensuring the transmission rate constraint. In Step 3, the starting and ending indices for the group with the smallest bit-flip probabilities are determined. Similarly, in Step 4, the indices for the group with the highest bit-flip probabilities are determined. In the subsequent steps, the modulation levels of

both groups are adjusted to minimize the total transmission power, as discussed in the earlier example. Specifically, in Step 7, the modulation levels corresponding to the low and high bit-flip probabilities, denoted as m_ℓ and m_h , are calculated. In Step 8, the adjusted modulation levels are computed by decreasing m_ℓ and increasing m_h . In Steps 9–12, the transmission power for each modulation level is determined by solving the BER equation, as done in the APC method. In Steps 13–25, the algorithm compares the total power of both groups to decide whether to adjust the modulation levels or keep them unchanged. If the decision is to maintain the current levels, the algorithm proceeds to the next groups. Here, the conditions for moving to the next groups are if adjusting the modulation levels increases the total power or if the modulation levels have reached their minimum or maximum values, denoted as m_{\min} and m_{\max} .

In the AMPC method, the procedure for determining the index of the most suitable encoder-decoder pair is the same as that in equation (34) of the APC method. Additionally, the optimized modulation level and power can be shared without any communication overhead because the AMPC method can be locally performed at the transmitter and receiver based on the pre-shared knowledge of $\{\mu^{(k)}\}_{\forall k}$.

The main advantage of the AMPC method is its ability to consistently achieve the same or lower total transmission power compared to the APC method. This is because the AMPC method starts with the same initial modulation level as the simple method, and then adjusts the modulation level toward minimizing power consumption. This advantage will be further validated through numerical simulations in Sec. V.

Remark 2 (Comparison with Conventional Modulation and Power Control Method): In traditional digital communication systems, modulation and power control methods are widely adopted to maximize spectral efficiency or minimize BER under varying channel conditions. One well-known method is the water-filling algorithm, which allocates more power to channels with higher SNR and less to those with lower SNR, maximizing spectral efficiency. Unlike these conventional methods, our framework differentiates itself by dynamically assigning different modulation and power to individual data bits, even when the channel conditions remain the same for all bits. This difference arises from the fact that conventional methods typically treat all data bits equally, without accounting for the varying levels of importance or sensitivity of each bit, whereas our framework recognizes that certain bits may be more critical for performing the receiver’s task. The performance gain of our strategy will be numerically demonstrated in Sec. V.

V. SIMULATION RESULTS AND ANALYSIS

In this section, we demonstrate the superiority of BlindJSCC, using the MNIST [25], CIFAR-10 [26], and STL-10 [27] datasets. The MNIST dataset consists of 70,000 grayscale images of handwritten digits, each of size 28×28 pixels, split into 60,000 training samples and 10,000 test samples. The CIFAR-10 dataset consists of 60,000 color images of size

TABLE II: The semantic encoder and decoder architectures for MNIST, CIFAR-10 and STL-10 datasets.

		Layers
MNIST	Encoder	C(32,3,1,2), PReLU, C(64,3,1,2), PReLU, C(64,5,2,1), PReLU, C(8,5,2,1)
	Decoder	CT(64,5,2,1,0), PReLU, CT(64,5,2,1,0), PReLU, CT(32,3,1,2,0), PReLU, CT(1,4,1,2,0)
CIFAR-10 / STL-10	Encoder	C(64,5,2,2), PReLU, C(128,5,2,2), PReLU, C(128,5,1,2), PReLU, C(128,5,1,2), PReLU, C(24,5,1,2)
	Decoder	CT(128,5,1,2,0), PReLU, CT(128,5,1,2,0), PReLU, CT(128,5,1,2,0), PReLU, CT(64,5,2,2,1), PReLU, CT(3,5,2,2,1)

$32 \times 32 \times 3$ pixels, split into 50,000 training samples and 10,000 test samples. The STL-10 dataset consists of 113,000 color images of size $96 \times 96 \times 3$ pixels, split into 105,000 training samples (including both labeled and unlabeled data) and 8,000 test samples.

Table II summarizes the semantic encoder and decoder architectures for each dataset, where the model architecture has been modified from that of [9] to improve task performance. In this table, $C(c,k,s,p)$ represents a 2D convolutional layer with c output channels, a $k \times k$ kernel, a stride of s , and padding of p . Similarly, $CT(c,k,s,p,p_o)$ denotes a transposed 2D convolutional layer with c output channels, a $k \times k$ kernel, a stride of s , padding of p , and output padding of p_o . In the training process, the number of epochs is set to 50, 100, and 200 for the MNIST, CIFAR-10, and STL-10 datasets, respectively. For all datasets, the batch size is set to 16, and the Adam optimizer in [36] is employed with an initial learning rate of 10^{-4} to train the semantic encoder and decoder. Additionally, for all datasets, the target transmission rate R_{target} and the total available transmission power P_{tot} are set to 4 and 100, respectively. The communication channel for all simulations is modeled as a Rayleigh fading channel.

In our simulations, we consider the following baselines for performance comparison:

- **BlindJSCC-P / BlindJSCC-MP:** These are the proposed digital DeepJSCC frameworks, where BlindJSCC-P only incorporates power control while BlindJSCC-MP employs both power control and adaptive modulation. In both methods, the number of encoder-decoder pairs is set to $K = 3$, and the loss function in (25) is employed with regularization weights $(\lambda_1, \lambda_2, \lambda_3) = (10^{-6}, 10^{-3}, 10^{-2})$. The bit-flip probabilities are uniformly initialized within the range of 0.01 to 0.49 and optimized using the Adam optimizer in [36] with an initial learning rate of 10^{-3} . In this framework, if the APC and AMPC methods fail to achieve the last K th bit-flip probability set, mainly due to the low total power or poor channel conditions, the optimized powers are adjusted by multiplying them with an appropriate constant to satisfy the total power constraint. For the AMPC method, the minimum and maximum modulation levels are set to 2 and 6, respectively.
- **NECST (Multi-bit):** This framework extends the quantization process of the digital DeepJSCC framework pre-

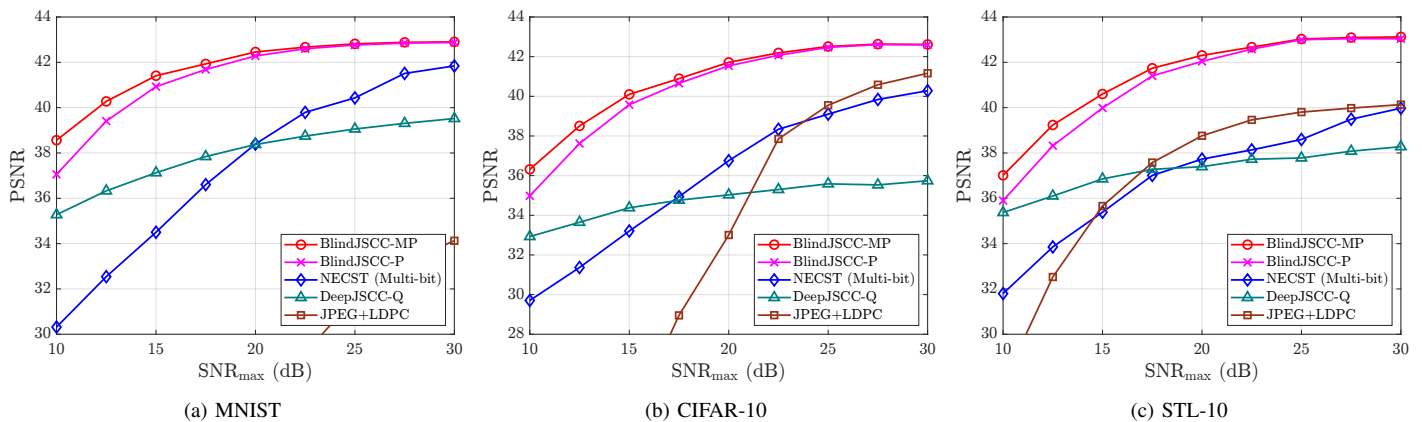


Fig. 5: Comparison of the PSNRs for various DeepJSCC and non-JSCC frameworks using MNIST, CIFAR-10, and STL-10 datasets.

sented in [14] from one-bit to multi-bit. During training, the framework employs multiple BSC in (15), with identical bit-flip probabilities applied to all channels. Consequently, the power and modulation levels are uniformly set across all symbols under the constraints on total power and transmission rate.

- **DeepJSCC-Q**: This is the digital DeepJSCC framework in [15], where the real-valued output of the encoder is mapped to discrete symbols. In this framework, the soft-to-hard quantizer described in [15] is employed. To match the symbol sequence length with that of other baselines, the output length of the encoder is adjusted by modifying the number of output channels in the last layer to 32 for the MNIST dataset and 96 for the CIFAR-10 and STL-10 datasets.
- **JPEG+LDPC**: This framework utilizes a separate source-channel coding, employing the joint photographic experts group (JPEG) for source coding and the 3/4-rate low-density parity-check (LDPC) code for channel coding. To ensure the transmission rate constraint, the modulation levels are adjusted between 2 and 10. Additionally, the JPEG quality settings are set to 80 for the MNIST dataset and 100 for the CIFAR-10 and STL-10 datasets, ensuring compliance with the transmission rate requirements.

In the BlindJSCC-P, BlindJSCC-MP and NECST frameworks, the encoder output is processed by the ReLU6 activation function, followed by an 8-bit uniform quantizer that discretizes values within the range of 0 to 6.

Fig. 5 compares the PSNRs of various frameworks across a range of SNR_{\max} levels in (8), using the MNIST, CIFAR-10, and STL-10 datasets. In this simulation, the maximum achievable SNR, denoted as SNR_{\max} , varies with the expected channel-gain-to-noise-power ratio, $\mathbb{E}[\gamma]$, while maintaining a fixed total available transmission power P_{tot} as 100¹. Fig. 5 shows that BlindJSCC-P and BlindJSCC-MP frameworks consistently achieves the highest PSNR across all SNR_{\max} levels. Notably, BlindJSCC-P and BlindJSCC-MP achieve these results

¹This scenario can be readily extended to various communication settings by multiplying P_{tot} and $\mathbb{E}[\gamma]$ by the constants $c > 0$ and $\frac{1}{c}$, respectively.

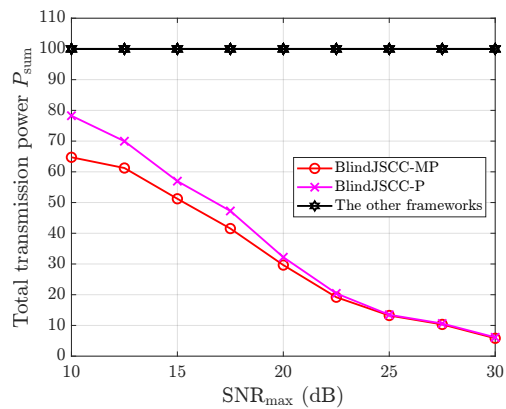


Fig. 6: Comparison of total transmission power between BlindJSCC-P, BlindJSCC-MP, and other frameworks at various SNR_{\max} levels using the CIFAR-10 dataset.

using only $K = 3$ encoder-decoder pairs, while other frameworks utilize 9 pairs trained for distinct SNR_{\max} levels. The performance comparison clearly indicates that BlindJSCC-P and BlindJSCC-MP consistently outperform the NECST framework, highlighting the superior effectiveness of the proposed error-adaptive blind training strategy. This is because, while the NECST framework applies a rigid constraint by enforcing a uniform bit-flip probability μ_n across all bits, BlindJSCC-P and BlindJSCC-MP relax this constraint by optimizing μ_n for each bit individually. This flexibility allows BlindJSCC-P and BlindJSCC-MP to better adapt to varying bit-reliability conditions, resulting in significantly improved performance. Further, the performance gap between BlindJSCC-P and BlindJSCC-MP shows the effectiveness of the AMPC method. This performance gap arises from the fact that the AMPC method operates with lower power consumption compared to the APC method, allowing it to effectively select the best-performing encoder-decoder pair, thus leading to superior overall performance. Meanwhile, the comparison with JPEG+LDPC highlights the limitations of separate source and channel coding, as it shows much lower PSNR, especially at low SNRs.

Fig. 6 compares the total transmission power of BlindJSCC-P and BlindJSCC-MP with that of other existing frame-

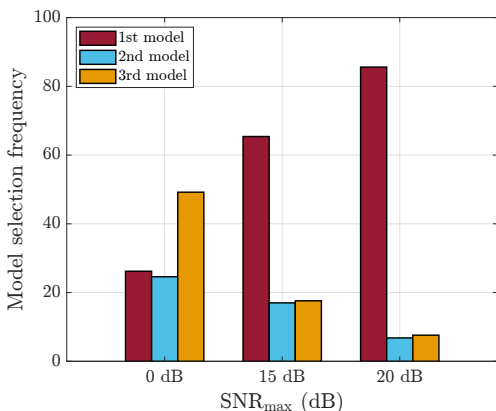


Fig. 7: Model selection frequency of the AMPC method across varying SNR_{max} levels on the CIFAR-10 dataset.

works across varying SNR_{max} levels, using the CIFAR-10 dataset. The corresponding PSNR performance is illustrated in Fig. 5(b). Note that all baseline frameworks, except BlindJSCC-P and BlindJSCC-MP, fully utilized the total available power P_{tot} . Nevertheless, the results clearly show that BlindJSCC-P and BlindJSCC-MP not only achieve higher PSNR across all SNR_{max} levels but also significantly reduce total power consumption. Within BlindJSCC, both the APC and AMPC methods are analyzed. The results show that the AMPC method consistently outperforms the APC method in terms of both PSNR and total transmission power, particularly at lower SNR_{max} levels. This highlights the superior efficiency of the AMPC method in low-SNR communication environments, demonstrating that dynamically optimizing both transmission power and modulation levels can provide better performance than adjusting transmission power alone.

Fig. 7 illustrates the model selection frequency of the proposed AMPC method across different SNR_{max} levels, using the CIFAR-10 dataset. Fig. 7 shows that at low SNR level of 0 dB, the third model is selected more frequently due to its higher average bit-flip probability, which is more likely to be achieved compared to the first and second bit-flip probability sets under poor channel conditions. As SNR_{max} increases to 15 dB and 20 dB, the frequency of selecting the third model decreases, and the first model becomes dominant. This smooth transition in model selection demonstrates the effectiveness of the AMPC method in adapting to varying SNR levels, ultimately ensuring higher task performance. Meanwhile, although the results of the APC method could not be included due to space constraints, the method also exhibits a similar adaptive behavior to the AMPC method under varying SNR levels.

Fig. 8 presents the modulation levels determined by both the APC and AMPC methods alongside the trained bit-flip probabilities. The simulation was conducted using the MNIST dataset with a trained K th bit probability set. Fig. 8 shows that the APC method applies a constant modulation level regardless of bit-flip probability. In contrast, in the AMPC method, as the bit-flip probability increases, the modulation level correspondingly rises. This result aligns with the core

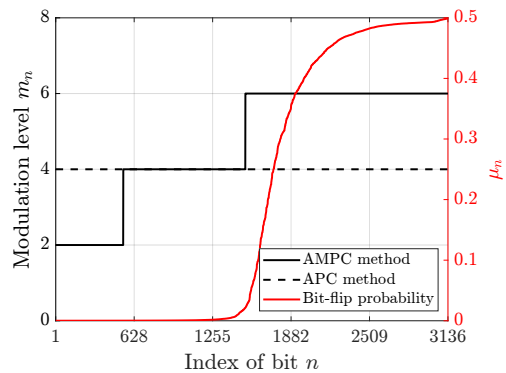


Fig. 8: Trained bit-flip probabilities and the modulation levels determined by the APC and AMPC methods on the MNIST dataset.

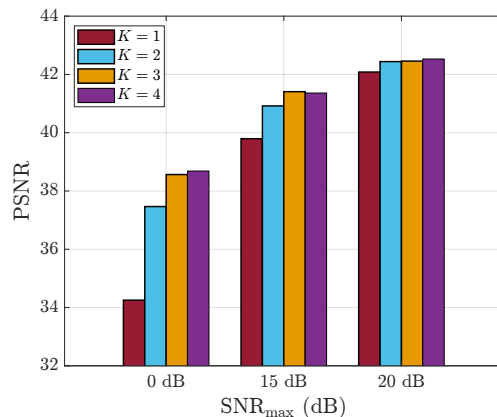


Fig. 9: Comparison of PSNR in BlindJSCC-MP for different numbers of encoder-decoder pairs K across varying SNR_{max} levels on the MNIST dataset.

principle of the AMPC method, as described in IV-C, where lower modulation levels are assigned to bits with lower bit-flip probabilities, and higher modulation levels are allocated to bits with higher probabilities. Consequently, by harnessing the potential performance gains from optimizing the modulation levels, the AMPC method reduces the total transmission power compared to the APC method, as shown in Figs. 5 and 6.

In Fig. 9, the PSNR of BlindJSCC-MP is compared for different numbers of encoder-decoder pairs, denoted as K , across varying SNR_{max} levels, using the MNIST dataset. In this simulation, the regularization weights are set as follows: $\lambda_1 = 10^{-6}$ for $K = 1$, $(\lambda_1, \lambda_2) = (10^{-6}, 10^{-3})$ for $K = 2$, $(\lambda_1, \lambda_2, \lambda_3) = (10^{-6}, 10^{-3}, 10^{-2})$ for $K = 3$, and $(\lambda_1, \lambda_2, \lambda_3, \lambda_4) = (10^{-6}, 10^{-4}, 10^{-3}, 10^{-2})$ for $K = 4$. Fig. 9 shows that as K increases, the PSNR also improves at all SNR_{max} levels. This improvement is attributed to the fact that increasing K enables the proposed framework to more densely represent diverse communication environments, allowing for finer adaptation to varying channel conditions. Fig. 9 also illustrates that the performance difference between $K = 3$ and $K = 4$ is minimal. This suggests that BlindJSCC-MP can achieve high task performance without requiring a large number of encoder-decoder pairs, enabling more efficient deployment in practical semantic communication systems.

VI. CONCLUSION

In this paper, we have proposed a novel digital DeepJSCC framework that effectively addresses the challenges of adapting to diverse communication environments. Unlike traditional DeepJSCC methods, our training strategy has eliminated the need for prior knowledge of the communication environment by treating bit-flip probabilities as trainable parameters. Additionally, our framework has introduced a training-aware communication strategy that dynamically selects the optimal encoder-decoder pair based on current channel conditions, ensuring efficient power usage while maintaining high performance. Simulation results have demonstrated that our framework significantly outperforms existing methods, achieving superior PSNR, lower power consumption, and greater adaptability with fewer encoder-decoder models. An important direction for future research is to develop an analytical method for determining the optimal number of models and λ_k values. Another promising research direction is to extend the proposed framework to incorporate more sophisticated modulation and coding schemes, further enhancing its performance.

REFERENCES

- [1] X. Luo, H.-H. Chen, and Q. Guo, "Semantic communications: Overview, open issues, and future research directions," *IEEE Wireless Commun.*, vol. 29, no. 1, pp. 210–219, Feb. 2022.
- [2] C. Chaccour, W. Saad, M. Debbah, Z. Han, and H. V. Poor, "Less data, more knowledge: Building next generation semantic communication networks," *IEEE Commun. Surveys Tuts.*, early access, Jun. 2024. doi: 10.1109/COMST.2024.3412852.
- [3] W. Yang, H. Du, Z. Q. Liew, W. Y. B. Lim, Z. Xiong, D. Niyato, X. Chi, X. Shen, and C. Miao, "Semantic communications for future Internet: Fundamentals, applications, and challenges," *IEEE Commun. Surveys Tuts.*, vol. 25, no. 1, pp. 213–250, firstquarter 2023.
- [4] H. Seo, J. Park, M. Bennis, and M. Debbah, "Semantics-native communication via contextual reasoning," *IEEE Trans. Cogn. Commun. Netw.*, vol. 9, no. 3, pp. 604–617, Jun. 2023.
- [5] J. Park, J. Choi, S.-L. Kim, and M. Bennis, "Enabling the wireless metaverse via semantic multiverse communication," in *Proc. IEEE Int. Conf. Sens. Commun. Netw. (SECON)*, Madrid, Spain, Sep. 2023, pp. 85–90.
- [6] D. Huang, F. Gao, X. Tao, Q. Du, and J. Lu, "Toward semantic communications: Deep learning-based image semantic coding," *IEEE J. Sel. Areas Commun.*, vol. 41, no. 1, pp. 55–71, Jan. 2023.
- [7] P. Jiang, C.-K. Wen, S. Jin, and G. Y. Li, "Wireless semantic communications for video conferencing," *IEEE J. Sel. Areas Commun.*, vol. 41, no. 1, pp. 230–244, Jan. 2023.
- [8] S. Wang, J. Dai, Z. Liang, K. Niu, Z. Si, C. Dong, X. Qin, and P. Zhang, "Wireless deep video semantic transmission," *IEEE J. Sel. Areas Commun.*, vol. 41, no. 1, pp. 214–229, Jan. 2023.
- [9] E. Bourtsoulatzé, D. Burth Kurka, and D. Gündüz, "Deep joint source-channel coding for wireless image transmission," *IEEE Trans. Cogn. Commun. Netw.*, vol. 5, no. 3, pp. 567–579, Sep. 2019.
- [10] D. B. Kurka and D. Gündüz, "DeepJSCC-f: Deep joint source-channel coding of images with feedback," *IEEE J. Sel. Areas Inf. Theory*, vol. 1, no. 1, pp. 178–193, May 2020.
- [11] W. Zhang, H. Zhang, H. Ma, H. Shao, N. Wang, and V. C. M. Leung, "Predictive and adaptive deep coding for wireless image transmission in semantic communication," *IEEE Trans. Wireless Commun.*, vol. 22, no. 8, pp. 5486–5501, Aug. 2023.
- [12] J. Xu, B. Ai, W. Chen, A. Yang, P. Sun, and M. Rodrigues, "Wireless image transmission using deep source channel coding with attention modules," *IEEE Trans. Circuits Syst. Video Technol.*, vol. 32, no. 4, pp. 2315–2328, Apr. 2022.
- [13] M. Rao, N. Farsad, and A. Goldsmith, "Variable length joint source-channel coding of text using deep neural networks," in *Proc. IEEE Int. Workshop Signal Process. Adv. Wireless Commun. (SPAWC)*, Kalamata, Greece, Aug. 2018, pp. 1–5.
- [14] K. Choi, K. Tatwawadi, A. Grover, T. Weissman, and S. Ermon, "Neural joint source-channel coding," in *Proc. Int. Conf. Machine Learning (ICML)*, Long Beach, CA, USA, Jun. 2019, pp. 1182–1192.
- [15] T.-Y. Tung, D. B. Kurka, M. Jankowski, and D. Gündüz, "DeepJSCC-Q: Constellation constrained deep joint source-channel coding," *IEEE J. Sel. Areas Inf. Theory*, vol. 3, no. 4, pp. 720–731, Dec. 2022.
- [16] Y. Bo, Y. Duan, S. Shao, and M. Tao, "Joint coding-modulation for digital semantic communications via variational autoencoder," *IEEE Trans. Commun.*, vol. 72, no. 9, pp. 5626–5640, Sep. 2024.
- [17] M. Wang, J. Li, M. Ma, and X. Fan, "Constellation design for deep joint source-channel coding," *IEEE Signal Process. Lett.*, vol. 29, pp. 1442–1446, Jul. 2022.
- [18] W. Li, H. Liang, C. Dong, X. Xu, P. Zhang, and K. Liu, "Non-orthogonal multiple access enhanced multi-user semantic communication," *IEEE Trans. Cogn. Commun. Netw.*, vol. 9, no. 6, pp. 1438–1453, Dec. 2023.
- [19] H. Xie and Z. Qin, "A lite distributed semantic communication system for Internet of things," *IEEE J. Sel. Areas Commun.*, vol. 39, no. 1, pp. 142–153, Jan. 2021.
- [20] S. Xie, S. Ma, M. Ding, Y. Shi, M. Tang, and Y. Wu, "Robust information bottleneck for task-oriented communication with digital modulation," *IEEE J. Sel. Areas Commun.*, vol. 41, no. 8, pp. 2577–2591, Aug. 2023.
- [21] P. Vepakomma, O. Gupta, T. Swedish, and R. Raskar, "Universal joint source-channel coding for modulation-agnostic semantic communication," 2024, *arXiv:2405.10749*.
- [22] H. Gao, G. Yu, and Y. Cai, "Adaptive modulation and retransmission scheme for semantic communication systems," *IEEE Trans. Cogn. Commun. Netw.*, vol. 10, no. 1, pp. 150–163, Feb. 2024.
- [23] Q. Zhou, R. Li, Z. Zhao, Y. Xiao, and H. Zhang, "Adaptive bit rate control in semantic communication with incremental knowledge-based HARQ," *IEEE Open J. Commun. Soc.*, vol. 3, pp. 1076–1089, Jul. 2022.
- [24] J. Park, Y. Oh, S. Kim, and Y.-S. Jeon, "Joint source-channel coding for channel-adaptive digital semantic communications," *IEEE Trans. Cogn. Commun. Netw.*, early access, Jul. 2024.
- [25] Y. Lecun, L. Bottou, Y. Bengio, and P. Haffner, "Gradient-based learning applied to document recognition," *Proceedings of the IEEE*, vol. 86, no. 11, pp. 2278–2324, Nov. 1998.
- [26] A. Krizhevsky, "Learning multiple layers of features from tiny images," M.S. thesis, Univ. Toronto, Toronto, ON, Canada, 2009.
- [27] A. Coates, A. Ng, and H. Lee, "An analysis of single-layer networks in unsupervised feature learning," in *Proc. Int. Conf. Artif. Intell. Statist. (AISTATS)*, Fort Lauderdale, FL, USA, Apr. 2011, pp. 215–223.
- [28] Y. Oh, J. Park, J. Choi, J. Park, and Y.-S. Jeon, "Power control after blind training for channel-adaptive digital deep joint source-channel coding," submitted to *IEEE Int. Conf. Commun. (ICC)*.
- [29] A. Goldsmith, "Capacity of wireless channels," in *Wireless communication*. Cambridge, U.K.: Cambridge Univ. Press, 2005.
- [30] Y. Oh, J. Lee, C. G. Brinton, and Y.-S. Jeon, "Communication-efficient split learning via adaptive feature-wise compression," 2023, *arXiv:2307.10805*.
- [31] R. Gray and D. Neuhoff, "Quantization," *IEEE Trans. Inf. Theory*, vol. 44, no. 6, pp. 2325–2383, Oct. 1998.
- [32] S. Ma, C. Zhang, B. Shen, Y. Wu, H. Li, S. Li, G. Shi, and N. Al-Dhahir, "Semantic feature division multiple access for multi-user digital interference networks," *IEEE Trans. Wireless Commun.*, early access, Jul. 2024.
- [33] K. Cho and D. Yoon, "On the general BER expression of one- and two-dimensional amplitude modulations," *IEEE Trans. Commun.*, vol. 50, no. 7, pp. 1074–1080, Jul. 2002.
- [34] C. J. Maddison, A. Mnih, and Y. W. Teh, "The concrete distribution: A continuous relaxation of discrete random variables," in *Proc. Int. Conf. Learn. Represent. (ICLR)*, Toulon, France, Apr. 2017, pp. 1–20.
- [35] E. Süli and D. F. Mayers, "Solution of equations by iteration," in *An introduction to numerical analysis*. Cambridge, U.K.: Cambridge Univ. Press, 2003.
- [36] D. P. Kingma and J. Ba, "Adam: A method for stochastic optimization," in *Proc. Int. Conf. Learn. Represent. (ICLR)*, San Diego, CA, USA, May 2015, pp. 1–13.